AFRL-AFOSR-VA-TR-2019-0345

Metasurface Polarimetry

Kristjan Leosson
Nyskopunarmidstod Islands

11/07/2019
Final Report

Air Force Research Laboratory
AF Office Of Scientific Research (AFOSR)/ RTA1
Arlington, Virginia 22203
Air Force Materiel Command

DISTRIBUTION A: Distribution approved for public release.

REPORT DOCUMENTATION PAGE

Form Approved
OMB No. 0704-0188

1. REPORT DATE *(DD-MM-YYYY)*	2. REPORT TYPE	3. DATES COVERED *(From - To)*
15-11-2019	Final Performance	15 Feb 2016 to 14 Feb 2019

4. TITLE AND SUBTITLE
Metasurface Polarimetry

5a. CONTRACT NUMBER

5b. GRANT NUMBER
FA9550-16-1-0136

5c. PROGRAM ELEMENT NUMBER
61102F

6. AUTHOR(S)
Kristjan Leosson

5d. PROJECT NUMBER

5e. TASK NUMBER

5f. WORK UNIT NUMBER

7. PERFORMING ORGANIZATION NAME(S) AND ADDRESS(ES)
Nyskopunarmidstod Islands
Keldnaholti
Reykjavik, 112 IS

8. PERFORMING ORGANIZATION REPORT NUMBER

9. SPONSORING/MONITORING AGENCY NAME(S) AND ADDRESS(ES)
AF Office of Scientific Research
875 N. Randolph St. Room 3112
Arlington, VA 22203

10. SPONSOR/MONITOR'S ACRONYM(S)
AFRL/AFOSR RTA1

11. SPONSOR/MONITOR'S REPORT NUMBER(S)
AFRL-AFOSR-VA-TR-2019-0345

12. DISTRIBUTION/AVAILABILITY STATEMENT
A DISTRIBUTION UNLIMITED: PB Public Release

13. SUPPLEMENTARY NOTES

14. ABSTRACT
In collaboration with the research group of Prof. F. Capasso at Harvard University, the PIs research group demonstrated polarization-dependent scattering from a single metasurface that cast the polariza-tion state of the input light into a number of intensity measurements [1,2], forming the theoretical basis for the present project. Metasurfaces designed to provide four or more sufficiently independent scatter-ing signals can be characterized as full Stokes polarimeters. Generally speaking, a full Stokes polarime-ter is a device that performs measurements of all four Stokes parameters describing the state and degree of polarization of electromagnetic waves, as well as their intensity. With current technology, this is typically achieved using either a wavefront-division, time-division or intensity-division approach. An in-line polarimeter performs such measurements by using only a fraction of the light intensity to measure the full state of polarization, preferably without significantly perturbing the input polarization. In-line intensity-division polarimeters are important, for example, for polarization generation and polarization management in optical telecommunications. The main task of the present project was to design and realize noval stand-alone polarimeter devices based on polarization-dependent scattering from metasur-faces, in addition to determining their performance and robustness

15. SUBJECT TERMS
metasurface, polarimetry

16. SECURITY CLASSIFICATION OF:			17. LIMITATION OF ABSTRACT	18. NUMBER OF PAGES	19a. NAME OF RESPONSIBLE PERSON
a. REPORT	b. ABSTRACT	c. THIS PAGE			POMRENKE, GERNOT
Unclassified	Unclassified	Unclassified	UU		

Standard Form 298 (Rev. 8/98)
Prescribed by ANSI Std. Z39.18

				19b. TELEPHONE NUMBER *(Include area code)* 703-696-8426

AIR FORCE OFFICE OF SCIENTIFIC RESEARCH

Project Title:	**Metasurface Polarimetry**
Principal investigator:	Kristjan Leosson, Innovation Center Iceland
AFOSR Grant No.:	FA9550-14-1-0389 and FA9550-16-1-0136
Project Period:	04/01/2016-03/31/2019
Date:	30 June 2019
Program Officer:	Gernot Pomrenke

Students and Postdoctoral Fellows funded by FA9550-14-1-0389

Michael Juhl, Ph.D. student

Dr. J.P. Balthasar Mueller, Postdoctoral Fellow

Dr. Einar B. Magnusson, Postdoctoral Fellow

Student funded by FA9550-16-1-0136

Michael Juhl, Ph.D. student

1. Aim

The overall aim of the proposed project was to introduce a disruptive technique of polarization analysis using polarization-sensitive metasurfaces. We have sought to develop a thorough understanding of the scattering properties of polarization-sorting metasurfaces. Based on this work, we have generated new device designs for full Stokes vector characterization of incident light in a transmission (in-line) geometry and developed new approaches to calibrating such optical devices, using a neural network approach.

2. Research Background

In collaboration with the research group of Prof. F. Capasso at Harvard University, the PI's research group demonstrated polarization-dependent scattering from a single metasurface that cast the polarization state of the input light into a number of intensity measurements [1,2], forming the theoretical basis for the present project. Metasurfaces designed to provide four or more sufficiently independent scattering signals can be characterized as full Stokes polarimeters. Generally speaking, a full Stokes polarimeter is a device that performs measurements of all four Stokes parameters describing the state and degree of polarization of electromagnetic waves, as well as their intensity. With current technology, this is typically achieved using either a wavefront-division, time-division or intensity-division approach. An in-line polarimeter performs such measurements by using only a fraction of the light intensity to measure the full state of polarization, preferably without significantly perturbing the input polarization. In-line intensity-division polarimeters are important, for example, for polarization generation and polarization management in optical telecommunications. The main task of the present project was to design and realize noval stand-alone polarimeter devices based on polarization-dependent scattering from metasurfaces, in addition to determining their performance and robustness.

3. Project Timeline

In the first project year, in-line polarimeters were fabricated and their scattering properties were investigated, both in an in-plane and an out-of-plane geometry [3]. In both cases, a linear matrix transformation was used to map four intensity measurements of the metasurface polarimeters back to the Stokes vector of the incoming light. A distinct limitation of this approach is that the device matrix is highly wavelength-dependent. Hence, polarization can only be accurately determined by the linearly calibrated metasurface polarimeter if the input wavelength is within approximately 0.1 nm of the calibration wavelength. This limitation can, in principle, be addressed by deploying a highly-resolved look-up table containing device matrices for each wavelength, provided also that the input wavelength is known with sufficient accuracy. Given the potential size of such a table, and that wavelength information may not be available, a calibration method that enables wavelength-independent polarimetry within a given range is highly desirable.

Considering its importance, the issue of solving the wavelength dependence of the metasurface polarimeters was given high priority in the 2nd project year, in addition to the previously planned tasks, listed in the 1st annual report: (a) Demonstration of fast sampling, (b) achieving proper control over device vectors, (c) reducing alignment sensitivity, (d) testing a 6-output metasurface geometry, and (e) constructing a partial polarization setup to evaluate DOP response. In an attempt to solve the wavelength dependence issue, it was decided to investigate the potential advantages of machine learning methods over traditional linear methods, as will be discussed in more detail below.

Increasing the sampling speed (a) and increasing the number of metasurface polarimeter outputs from four to six (d) was instrumental in allowing us to test a fundamentally new way of calibrating the device response, based on deep neural networks (DNNs). Our research showed that control over device vectors (b) was of secondary importance, as long as they remain sufficiently independent from each other, and that device response to variations in DOP (e) could be emulated by introducing SOP variations that were faster than the device response, as an alternative to constructing a dedicated setup [4].

Item (c) was addressed in Year 3 of the project, where metasurface polarimeters were fabricated directly on fiber facets, thus eliminating any possibility of alignment sensitivity.

4. Device fabrication and measurement setup

Packaged fiber-coupled metasurface polarimeters (Fig. 1), consisting of arrays of metal nanoantennas, were fabricated in Year 1 using electron-beam lithography for patterning periodic gold nanostructures on transparent substrates, as described in more detail in Ref. [3]. Analytical and numerical calculations were carried out, and two classes of polarimeters (in-plane and out-of-plane) having a four-port polarimeter functionality were fabricated and tested. For the packaged polarimeters, we compared two different geometries where four detectors pick up the light diffracted either in the plane of the metasurface (in-plane device) or at approximately 50° angle from the metasurface (out-of-plane device). The latter design proved less sensitive to alignment of the incident radiation but exhibited a larger polarization-insensitive intensity component, reducing the dynamic range of the polarimeter. An antenna configuration providing polarization-dependent scattering into six directions (Fig. 2(b)) was realized in Year 2, yielding six device vectors. The six-output metasurface was fabricated in in-plane as well as out-of-plane polarimeter configurations. The orientations of the device vectors of an out-of-plane device are depicted on the Poincaré sphere in Fig. 2(c). The measurement setup (Fig. 3), constructed within Year 1, consisted of a tunable fiber-coupled laser, combined with a deterministic polarization controller, producing light with tunable input polarization, power and wavelength. The metasurface was positioned at the output end of the fiber and surrounded by photodetectors, as illustrated schematically in Fig. 2(a).

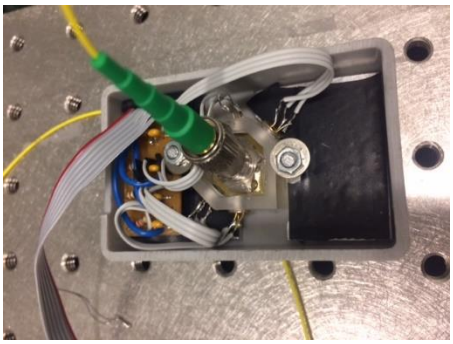

Fig. 1. Packaged fiber-coupled prototype device.

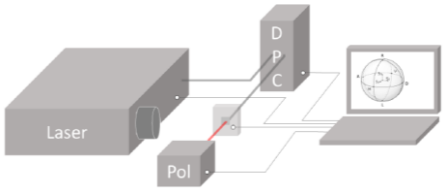

Fig. 3. Measurement setup schematic.

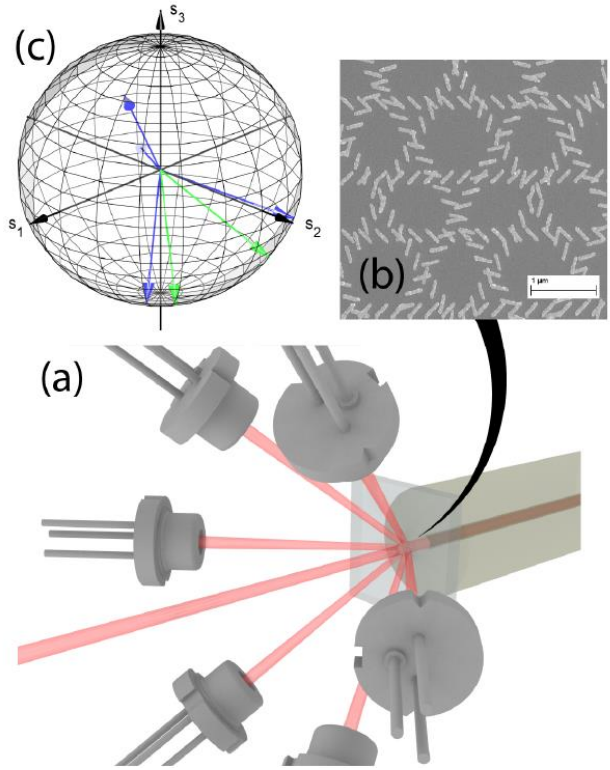

Fig. 2. (a) Device setup. (b) Electron micrograph of the metasurface layout. (c) Device vectors depicted on the Poincaré sphere.

The signal from the diodes was amplified and simultaneously sampled from all detectors, using a microcontroller. For reference, the light transmitted through the device was measured using a conventional time-division rotating-waveplate polarimeter.

5. Metasurface polarimeter on a fiber facet

In-line fiber-based polarimeters play a critical role in monitoring and controlling the polarization in optical communication networks. Current in-line polarimeters are typically based on scattering from two sets of tilted Bragg gratings inscribed in the fiber, separated by a polarization-rotating fiber section. Integrating a metasurface polarimeter on an optical fiber would therefore not only represent an important step towards the ultimate miniaturization of an in-line polarimeter device with potential applications, e.g., in optical networks. In order to realize a metasurface polarimeter on a fiber facet, a new pattern transfer method based on template stripping [5] was developed within the present project. The method is illustrated in Fig. 4. A mechanically cleaved fiber tip was dipped in a UV-curable hybrid organic/inorganic polymer leaving a droplet of polymer on the fiber tip. The fiber tip was then brought into near proximity to a gold nanopatterned silicon wafer bringing the droplet in contact with the sample (Fig. 4(a)). The polymer was then cured with 365-nm ultraviolet light using one of two approaches. With the fiber exposure approach the UV-light was transmitted through the fiber itself, thus forming a cylindrical polymer rod between the fiber and the wafer as a result of confinement within the fiber and a self-guiding phenomenon within the optically-cured polymer. After UV exposure, the fiber was retracted, delaminating the gold from the wafer and transferring it to the surface of the cured polymer rod, as a result of low adhesion between gold and silicon. UV-curing through the fiber ensures that the nanostructure is automatically transferred only to the area corresponding to the fiber core (Fig. 4(b)). Figure 4(c) illustrates an alternative flood-exposure approach where the polymer was cured from outside the fiber, thus curing the entire droplet of polymer on the fiber tip. The metasurfaces transferred to the polymer

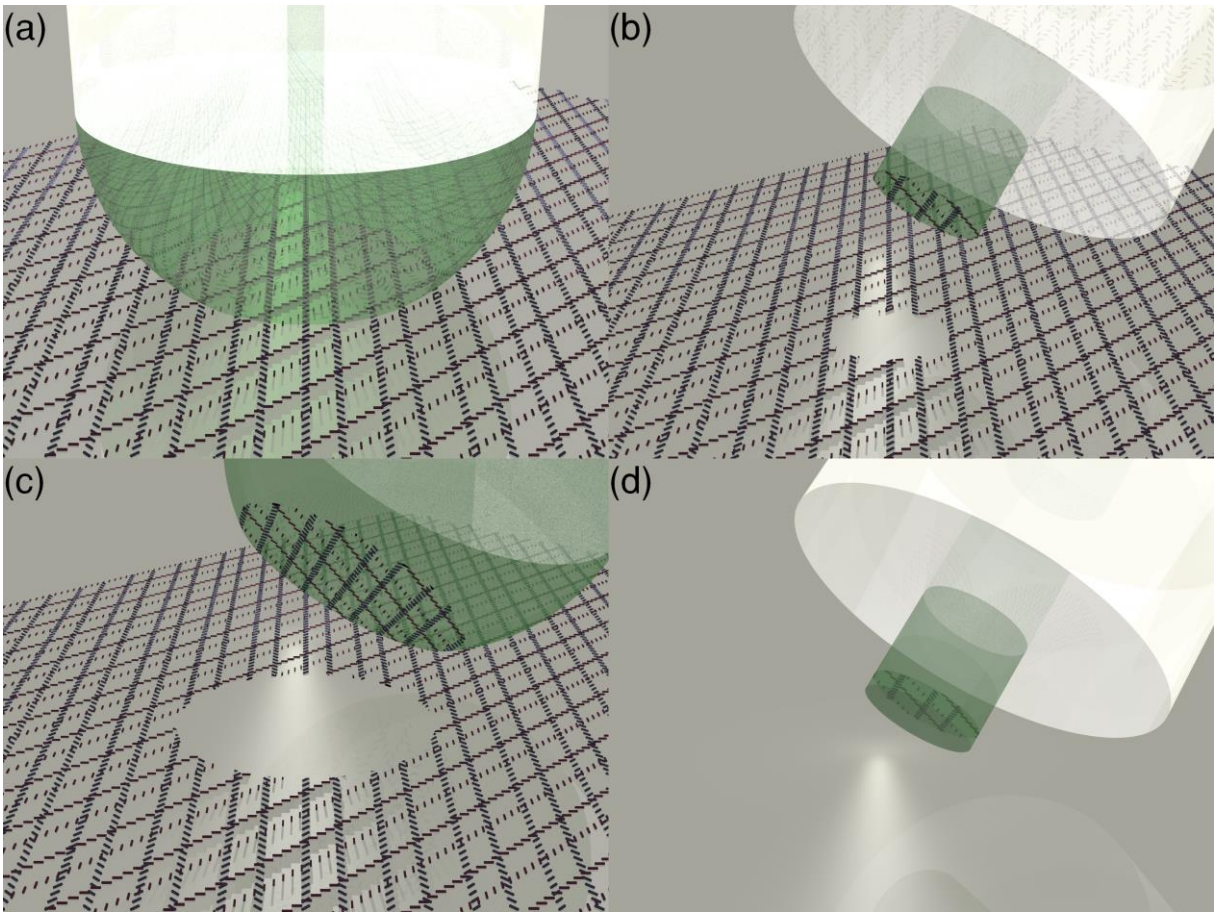

Fig. 4. (a) An optical fiber (white cylinder) with a drop of polymer (green hemisphere) on the tip in proximity to a metasurface consisting of arrays of gold nanoantennas. The metasurface is made of two superimposed gratings of antenna columns arranged in a pattern where the antennas in each column are rotated 90° relative to antennas in the neighboring column. (b) The polymer is UV-cured through the fiber core resulting in only the antennas under the center of the fiber being released from the wafer. (c) The polymer is UV-cured using flood exposure resulting in a larger metasurface area being released from the surface. (d) A second layer of polymer is cured on top of the existing polymer. The polymer is cured on an unstructured surface to ensure a flat end face.

rod can subsequently be fully embedded in polymer by repeating the process using a clean silicon wafer without nanoantennas. This is illustrated in Fig. 4(d) with the fiber exposure approach.

Electron micrograph images of the patterned fibers are shown in Fig. 5. The diameter of the polymer rod in Fig. 5(a) is 10–10.5 μm corresponding well to the core size of an SMF-28 optical fiber. The results of polarization measurements with a polarimeter using the fiber exposure method is shown in Fig. 6. Since the accuracy obtained with the polarimeter integrated on a fiber facet is the same as obtained with a wafer-based packaged polarimeter using the same metasurface design [6], it was concluded that the template stripping transfer lithography method is an effective method for fabricating high quality optical components and that a fiber-based metasurface in-line polarimeter is a viable alternative to conventional fiber-based in-line polarimeters. The pattern transfer technique described above is furthermore applicable to other situations where it is desired to transfer patterned metal nanostructures onto fiber facets, with possible auto-alignment to the fiber core.

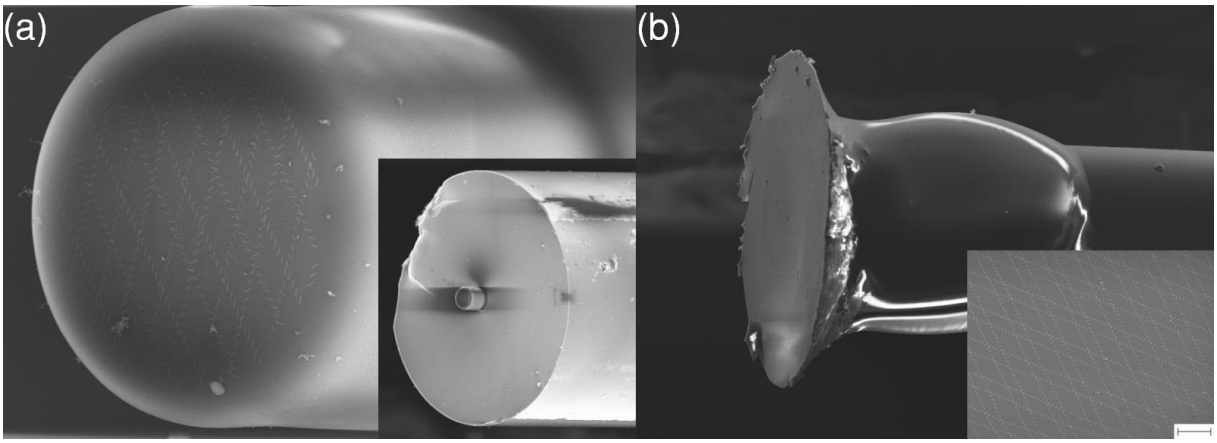

Fig. 5. Micrograph images of patterned fibers. (a) Image of a polarimeter fabricated with the fiber exposure approach, showing the 10 µm-diameter polymer rod with gold nanoantennas on the top. The inset shows a zoom-out of the entire fiber tip that has a cladding diameter of 125 µm. (b) Image of a patterned fiber facet using the flood exposure approach, where a much larger area of nanoantennas arrays is transferred. The inset shows a zoom-in of the transferred nanoantenna arrays imaged on the fiber facet (the scale bar represents a length of 2 µm).

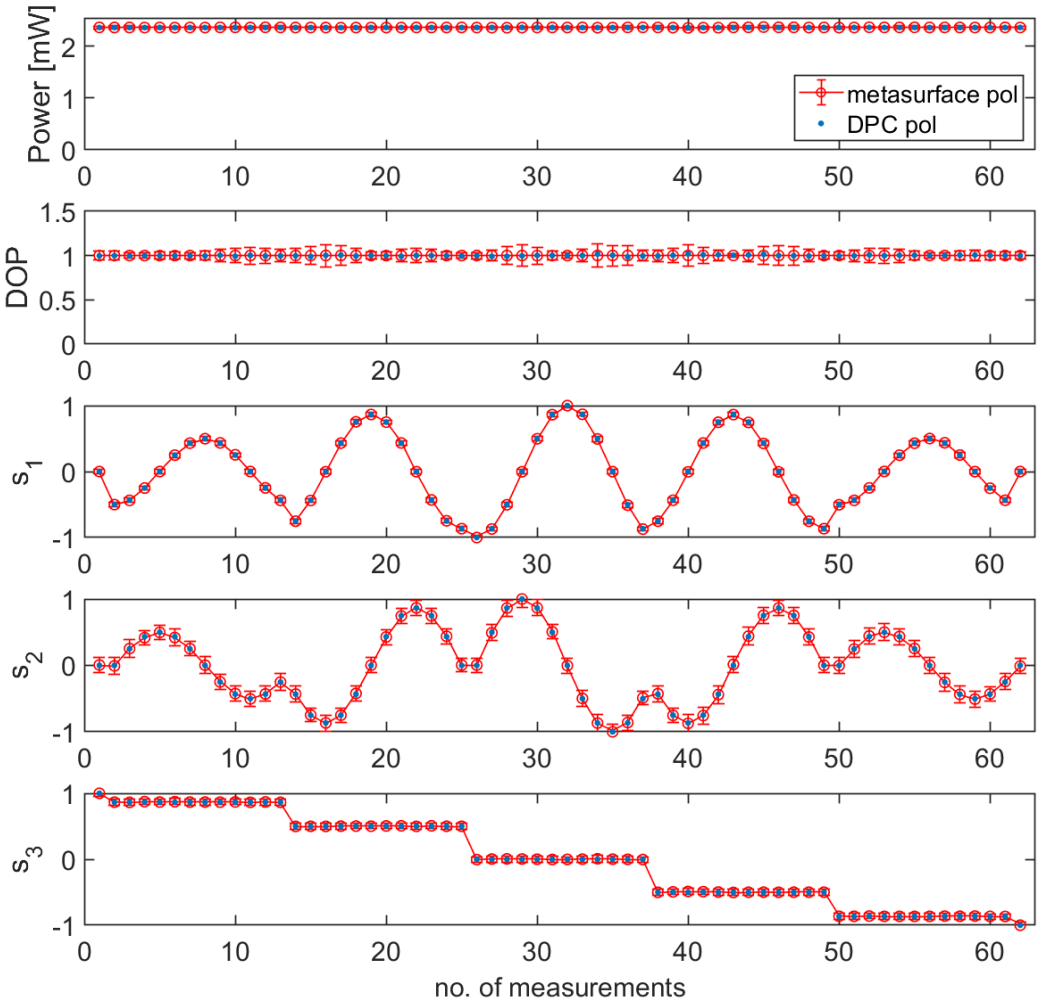

Fig. 6. Polarization measurements at 1550 nm using the fiber-based flood exposure metasurface polarimeter. The first subplot is the power of the incident light, which is proportional to the first element of the Stokes vector, S_0. The next subplot is the degree of polarization (DOP) and the three last subplots are the parameters characterizing the state of polarization (SOP), $s_1 - s_3$. The red circles are the polarization measurements of the metasurface polarimeter, the blue dots are the reference polarizations set by the deterministic polarization controller (DPC).

6. Linear vs. neural-network calibration

Traditionally in optical measurements, the reconstruction of relevant information in the input light field is frequently carried out by determining the inverse of a transfer matrix **T** (also referred to as the device matrix, instrument matrix, analysis matrix or transmission matrix) that maps an input vector **S** to an output vector **I**, where the latter typically consists of a set of intensity measurements, i.e. **I** = **T S**. The determination of the matrix inverse is non-trivial in the presence of experimental noise and the accuracy of the recovery of the original signal depends on the properties of the so-called device vectors (rows of the device matrix) [7,8]. In the case of the polarimeter devices described above, the inverse of the transfer matrix was determined from a large number of polarizations and intensities by taking the pseudo-inverse of the intensities [9]. The uncertainties of the polarization measurements where found by calculating the error propagation and a model for the systematic error was developed. Details of error and uncertainties as well as an in-depth investigation of wavelength dependence, device vector dependence and geometrical variation can be found in Ref. [10]. Even though device vectors were shown to be dependent on a number of factors, the six-output design proved to provide sufficiently independent device vectors and accuracies close to the specs of commercial polarimeters were obtained [10]. Nevertheless, a non-linear calibration method was introduced to address the limitation of the wavelength dependence of the linear calibration (see section 6).

Recent breakthroughs in machine learning (ML) techniques based on deep neural networks (DNNs) have transformed many information processing tasks, including game playing, computer vision and natural language translation [11,12]. Artificial neural networks represent a sub-class of computational architectures that include a large variety of non-linear statistical models and learning methods, first originating in attempts to simulate the human brain [13,14]. The most widely used neural networks define a mapping between a set of input variables and a set of output variables, based on a sequence of linear transformations followed by nonlinear activation functions that form the layers of a network. It has been shown that neural networks with a single hidden layer are universal function approximators, i.e., they can approximate continuous functions on a compact space. How to learn this representation from data is a non-trivial subject and currently an active area of research. In the case of regression, where the task is to learn a functional mapping to a space of continuous target variables, the general approach is to define a cost function (most commonly mean squared error), and work towards minimizing the cost while at the same time controlling for overfitting. This is most often done using gradient descent algorithms, which in the context of artificial neural networks is known as backpropagation. Although neural networks and backpropagation methods have been studied for decades [15], they have recently shown great success and potential due to increases in computing power and new techniques to make the model learning tractable, notably when the number of hidden layers is increased (`deep learning'). Previously, neural networks have been used for a variety of signal processing tasks based on sensor and imaging data [16-18].

7. Calibration Performance

At a particular input wavelength, the underlying optical physics determines that the relationship between the Stokes vector and the metasurface outputs is given by a simple projection, which is a linear transformation. We therefore considered the accuracy of the polarization measurement obtained using the device matrix for a given wavelength to represent a benchmark of the irreducible error of the polarimeter device at that wavelength. This error is related to instrument noise and the configuration of the device vectors. We determined the reference device matrices from the full sets of measured polarization states at each input wavelength using standard methods [3]. For our neural network calibration we used neural networks with one or more hidden layers where each layer was fully connected, i.e. where each node in a layer is defined by a linear combination of all the nodes in the previous layer. Every node in the hidden layers is activated with a nonlinear activation function, which we empirically chose as the exponential-

linear unit (ELU) [19] as this resulted in less noisy training curves than other commonly used activation functions. The models were trained using the ADAM optimization algorithm [20].

The investigated wavelength range covered the full telecom C-band (1530-1565 nm) in steps of 0.2 nm. For each value of the incident wavelength, a set of 100 polarization measurements was collected; each corresponding to a random polarization state. In order to eliminate artificial correlations arising e.g. from polarization-dependent insertion loss to the fibers, or depolarization in the system, the laser power in the training set was randomized, varying between 1-3 mW. The setup was automated to allow rapid collection of the large data sets required for neural network training with the desired variation of input parameters. The full dataset of 17,500 points was randomly split into training/validation/test sets in the ratio 3:1:1.

The accuracy of Stokes vector predictions from the metasurface polarimeter using different calibration models is summarized in Fig. 7. It shows the angular error of a single linear model applied to data from the full wavelength range (blue curve) as well as a model where the device is calibrated only at a wavelength of 1550 nm (black curve), compared to the result of using a separate linear model for each wavelength (green curve). The figure confirms that calibrating the device at a single wavelength only yields reliable results in a very narrow wavelength interval, while trying to generalize a single device matrix to the full wavelength range results in essentially random Stokes vector predictions from the measured data (angular error approaching 90°). The angular error obtained when a device matrix determined for each measured wavelength, on the other hand, is around 1°, representing the irreducible error for this particular metasurface, detector configuration, and measurement method.

The angular error obtained when applying the neural network model to the test data is also shown (red curve). The average error in this case is about 2.1°, which is only a factor of 2 higher than the benchmark error. For simplicity, we restricted optimization to modifying only the number of hidden layers and number of units per layer of the network (see below).

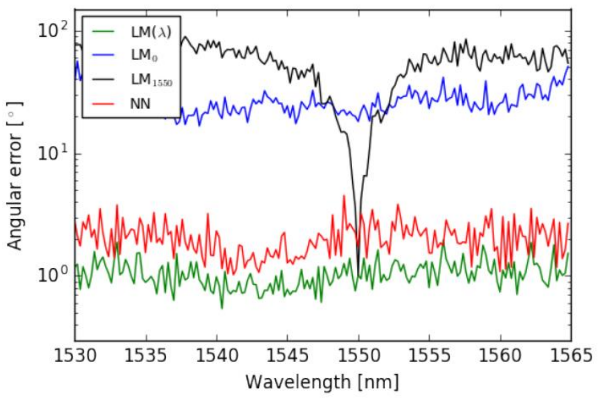

Figure 7. Comparison of the angular error of Stokes vector prediction using a linear transformation at each wavelength (green curve), a linear transformation without knowledge of wavelength (blue curve), a linear model fitted at a single wavelength (black curve), and a neural network with 7 hidden layers of 32 units each (red curve).

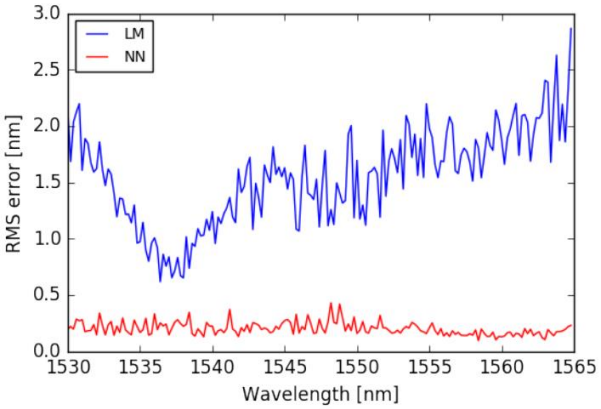

Figure 8. Comparison of wavelength modelling using a linear model (LM, blue curve) and a neural network (NN, red curve).

8. Metasurface Polarimeter achieves Wavemeter Functionality

Although the metasurface polarimeter devices were designed to measure polarization only, we considered also whether their inherent wavelength dependence would allow a neural network to determine the wavelength of the incoming (monochromatic) light from the measured data, thus adding a wavemeter functionality to the polarimeter device. Similarly to before, we fitted a linear model and trained a neural network on the 6-port metasurface polarimeter data for this task. Results are shown in Fig. 8, where a neural network with 3 hidden layers and 32 units per layer was used. The linear model (blue curve) can be seen to have a rather poor RMS error in wavelength prediction of 1-3 nm. The neural network model (red curve), on the other hand, performs an order of magnitude better, with an RMS error of 0.1-0.3 nm. It is worth mentioning that this error value is of the same order as the wavelength spacing used in the training set (0.2 nm).

These results show that 6-port metasurface polarimeters, calibrated using deep neural networks, provide an accuracy in the Stokes vector measurement close to the minimum device error *without a priori knowledge of the input wavelength*, in addition to accurately predicting the input wavelength (presupposing, in this case, a monochromatic input). As mentioned above, in our previous work [2,3] we focused on the traditional four-output approach, where the four parameters of the Stokes vector are projected onto an output space of equal dimensionality. In order to compare the neural network calibration approach on such devices with the performance of the 6-port devices reported here, we also tried limiting our neural network training to the 4 ports of the present device that gave the most precise linear calibration (blue arrows in Fig. 2(c)), which is equivalent to training a neural network on the output of a 4-port device. We were not able to train a well-performing neural network for Stokes vector prediction in this case. Thus, using six (or possibly more) sufficiently independent outputs makes it significantly easier to train well-performing models.

9. DNN Optimization

For the machine learning-based calibration discussed above, we trained a neural network with 7 hidden layers of 32 units each, using data from the full wavelength range. This choice of parameters was based on an investigation of the hyperparameter space. The results obtained from each neural network configuration that was tested are compared in Fig. 9. As the networks grow in layers and units, the models begin to overfit the training data. We address this by aborting the training process as soon as the loss on the validation set begins to increase with respect to the loss on the training set. Between choosing a model with a reasonable amount of free parameters and good prediction performance, a model consisting of 7 hidden layers of 32 units was selected.

As mentioned before, one way of accurately calibrating the metasurface for a given wavelength range is to use a lookup table of linear calibrations at closely spaced wavelengths. This is, however, only useful when the wavelength of the measured light is known beforehand. Given that we can accurately determine the wavelength with a neural network model, this implies that we can also create a hybrid model by using the wavelength determined by the neural network to look up the corresponding linear calibration. A comparison of such a hybrid model to the full neural network model revealed that the hybrid model, in fact, performs nearly as well as the full neural network model, with an average error of about 2.6° on the polarization prediction.

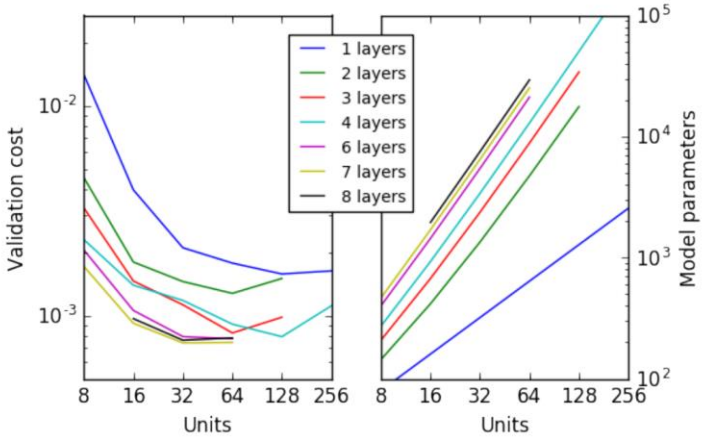

Figure 5. Optimizing neural network hyperparameters. Early stopping helps to avoid overfitting with high variance models, but the model performance saturates at around 7 hidden layers, 32 units per layer.

10. Conclusion

In summary, we have fabricated and tested packaged fiber-coupled metasurface polarimeters in in-plane and out-of-plane configurations, where individual photodetectors are placed directly in the path of the scattered light beams. The absence of optical elements between the metasurface and detectors makes packaging easier and allows for integrating the photodetector and metasurface on the same chip. Analytical models have been developed and compared to full-wave simulations to analyze the performance and error of the metasurface polarimeters. A new transfer-lithography process based on template stripping for nanostructuring of optical fiber facets was developed to realize the fabrication of a metasurface polarimeter integrated directly onto the facet of a standard single-mode telecom fiber (SMF28). The quality of the pattern transfer process was confirmed by comparing the performance of the fiber-integrated metasurface polarimeter to a wafer-based polarimeter. Measurements showed that the accuracy is not negatively affected by the transfer of the patterned gold nanostrutures from a wafer to an optical fiber facet.

We maintain that machine learning models, provided with a sufficient amount of calibration data, can be brought to interpret the input signals of an optical sensor in terms of functions that would be difficult or impossible to derive by hand. This can produce a much better approximation to the physics that determines the relationship between sensor input and output, but sacrifices an interpretable link between the physics and the calibration function. In case of the metasurface polarimeter, neural network models have enabled us to ameliorate the high sensitivity of the polarimeter to discrepancies between the input and the calibration wavelength, and also to extend its functionality to act as a wavemeter. Our results demonstrate the potential for this type of machine learning in producing substantial performance improvements of even relatively simple optical systems that have previously been treated in terms of transfer function matrix formalism. We believe that this general result can extend far beyond the polarimetry concept discussed within the present project.

11. Further work

Following up on the results of the present project, the work on neural optics will be expanded. Based on the experiences from the last three years we will fabricate neural polarimeters based on disordered photonic materials. Initial results show that using random materials it is relatively simple to increase the number of outputs, thereby increasing the accuracy considerably. Furthermore, we will show that deep

learning has the potential not only to solve the polarimeter's dependence on wavelength but also its sensitivity to mechanical vibrations and displacements.

12. Exchange grant (FA9550-16-1-0136)

Within project year 2, Ph.D. student Michael Juhl spent several months in the group of Prof. F. Capasso at Harvard University. Together with Ph.D. student Noah Rubin, he conducted measurements on parallel polarization state generation and measurement using dielectric metasurfaces. This exchange proved highly productive and resulted in a publication in Optics Express and a conference presentation (see below).

13. Project dissemination

Dissemination of the project included the following publications/presentations:

Michael Juhl, Carlos Mendoza, JP Balthasar Mueller, Federico Capasso, Kristjan Leosson, *Performance characteristics of 4-port in-plane and out-of-plane in-line metasurface polarimeters*, Optics Express 25, 28697-28709 (2017)

Noah A Rubin, Aun Zaidi, Michael Juhl, Ruo Ping Li, JP Balthasar Mueller, Robert C Devlin, Kristján Leósson, Federico Capasso, *Polarization state generation and measurement with a single metasurface*, Optics express 26, 21455-21478 (2018)

Einar B Magnusson, JP Balthasar Mueller, Michael Juhl, Carlos Mendoza, Kristjan Leosson, *Neural Polarimeter and Wavemeter*, ACS Photonics 5 (7), 2682-2687 (2018)

Michael Juhl, Jan Philipp Balthasar Mueller, Kristjan Leosson, *Metasurface Polarimeter on Optical Fiber Facet by Nano-Transfer to UV-Curable Hybrid Polymer*, IEEE Journal of Selected Topics in Quantum Electronics 25 (3), 1-7 (2019)

Jan Philipp Balthasar Mueller: *Polarization in Nanophotonics*, Ph.D. thesis, Harvard Applied Physics http://scholar.harvard.edu/jpbm/publications/polarization-nanophotonics (2016)

Michael Juhl, *Metasurface Polarimetry: Fabrication and Characterization of In-line Stokes Polarimeters Based on Polarization Sensitive Nanoantenna Arrays*, Ph.D. thesis, University of Iceland, School of Engineering and Natural Sciences, Faculty of Physical Sciences (2018)

Michael Juhl, Carlos Mendoza, JP Balthasar Mueller, Federico Capasso, Kristjan Leosson, *Packaged inline metasurface polarimeters with in-plane and out-of-plane detection*, Conference on Lasers and Electro-Optics Europe & European Quantum Electronics Conference (CLEO/Europe-EQEC, 2017)

Michael Juhl, Carlos Mendoza, JP Balthasar Mueller, Federico Capasso, Kristján Leósson, *Self-Aligned Nano-Transfer of Metasurface Polarimeter to an Optical Fiber Tip using UV-Curable Hybrid Polymer*, Conference on Lasers and Electro-Optics (CLEO, 2018)

Noah A Rubin, Aun Zaidi, Ruo Ping Li, Michael Juhl, Jan Phillipp Balthasar Mueller, Robert C Devlin, Kristjan Leosson, Federico Capasso, *Parallel polarization state generation and measurement with a single metasurface*, High Contrast Metastructures VIII 10928, 109280G (2019)

K. Leosson, Iceland's 350-Year Contribution to Optics, Opening Plenary Talk on Iceland Spar and polarimetry at DINAMO II, Siglufjordur, Iceland (2017).

References

[1] J.P. Balthasar Mueller, K. Leosson, F. Capasso, Nano Letters 14, 5524–5527 (2014)

[2] J.P. Balthasar Mueller, K. Leosson, F. Capasso, Optica 3, 42-47 (2016)

[3] M. Juhl, C. Mendoza, J.P.B. Mueller, F. Capasso, K. Leosson, Optics Express 25, 28697 (2017)

[4] N.A. Rubin, A. Zaidi, M. Juhl, R.P. Li, J.P.B. Mueller, R.C. Devlin, K. Leósson, F. Capasso, Optics express 26, 21455 (2018)

[5] P. Nagpal, N. C. Lindquist, S.-H. Oh, and D. J. Norris, Science 325, 594 (2009)

[6] M. Juhl, J. P. Balthasar Mueller, K. Leosson, IEEE Journal of Selected Topics in Quantum Electronics 25 (3), (2019)

[7] S.M. Popoff, G. Lerosey, M. Fink, A.C. Boccara, S. Gigan, New Journal of Physics 13, 123021 (2011)

[8] R.M.A. Azzam, JOSA A 20, 955-958 (2003)

[9] B. Boulbry, J. C. Ramella-Roman, and T. A. Germer, Appl. Opt. 46, 8533 (2007)

[10] Michael Juhl, Ph.D. thesis, University of Iceland (2018)

[11] D. Silver, et al. Nature 550, 354-359 (2017)

[12] Y. LeCun, Y. Bengio, G. Hinton, Nature 521, 436-444 (2015)

[13] J. Friedman, T. Hastie, R. Tibshirani, The elements of statistical learning; Springer series in statistics (NY 2001, Vol. 1)

[14] I. Goodfellow, Y. Bengio, A. Courville, Deep Learning; The MIT Press, 2016.

[15] J. Schmidhuber, Neural networks 61, 85-117 (2015)

[16] A. Moraru, M. Pesko, M. Porcius, C. Fortuna, D. Mladenic, J of Computing and Information Technology 18, 341 (2010)

[17] J. Xuan, U. Klimach, H. Zhao, Q. Chen, Y. Zou, Y. Wang, Intl. J. of Biomedical Imaging, 74143 (2007)

[18] T. Ando, R. Horisaki, J. Tanida, Optics Express 23, 33902 (2015)

[19] D.-A. Clevert, T. Unterthiner, S. Hochreiter, arXiv:1511.07289 (2015)

[20] D.P. Kingma, J.L. Ba, International Conference on Learning Representations 2015, 1-15 (2015)